Design and Implementation of Sparse Aperture Imaging Systems

Soon-Jo Chung*, David W. Miller**, Olivier L. de Weck***
Space Systems Laboratory, Massachusetts Institute of Technology
Cambridge, Massachusetts, 02139, USA

ABSTRACT

In order to better understand the technological difficulties involved in designing and building a sparse aperture array, the challenge of building a white light Golay-3 telescope was undertaken. The MIT Adaptive Reconnaissance Golay-3 Optical Satellite (ARGOS) project exploits wide-angle Fizeau interferometer technology with an emphasis on modularity in the optics and spacecraft subsystems. Unique design procedures encompassing the nature of coherent wavefront sensing, control and combining as well as various system engineering aspects to achieve cost effectiveness, are developed. To demonstrate a complete spacecraft in a 1-g environment, the ARGOS system is mounted on a frictionless air-bearing, and has the ability to track fast orbiting satellites like the ISS or the planets. Wavefront sensing techniques are explored to mitigate initial misalignment and to feed back real-time aberrations into the optical control loop. This paper presents the results and the lessons learned from the conceive, design and implementation phases of ARGOS. A preliminary assessment shows that the beam combining problem is the most challenging aspect of sparse optical arrays. The need for optical control is paramount due to tight beam combining tolerances. The wavefront sensing/control requirements appear to be a major technology and cost driver.

Keywords: sparse aperture, multiple-aperture optical systems, fizeau interferometer, phased telescope array

1. INTRODUCTION

The quest for finer angular resolution in astronomy will inevitably lead to larger apertures. Unfortunately, the primary mirror diameter for space telescopes is limited by volume and mass constraints of current launch vehicles as well as the scaling laws of manufacturing costs[1]. Since the cost of monolithic optics increases faster than diameter squared, and mirrors such as the Hubble Space Telescope's are already at the edge of what is financially feasible, efforts are ongoing to break this trend by employing breakthrough technologies such as deployed segmented mirror telescopes, and sparse aperture optics using interferometry. Whereas long baseline stellar Michelson interferometers feed lights from independent collectors to a beam combiner to obtain interfered fringes over a period of time, Fizeau interferometers produce a direct image with full instant u-v coverage. Hence, Fizeau interferometers are suitable for optical imaging of extended objects and rapidly changing targets. In contrast to the long baselines of Michelson interferometers, Fizeau interferometry systems tend to have compact telescope arrays. An optimal imaging configuration designed for sparse arrays was first proposed by Golay[2]. Sparse arrays are promising for applications that do not require extremely high sensitivity (bright source present) and allow for a rather limited field-of-view (FOV)[3,5]. A notable project in the area of phased telescope array is the Multipurpose Multiple Telescope Testbed (MMTT)[6] by Air Force Research Laboratory (AFRL). The MMTT consists of four 20-cm-aperture telescopes phased together with a 15-arcmin Field-of-View (FOV). The MMTT employs a complex laser interferometer metrology to sense wavefront error (WFE). The Multi Aperture Imaging Array[7] built by Lockheed Martin demonstrated phase diversity computation techniques for WFE sensing. This sparse array consists of afocal telescopes arranged in a Y-formation that are combined to a common focus in a Fizeau interferometer configuration. It demonstrated the first results of a broad band multiple telescope imaging array phased over a significant field of view using the extended image projector in the lab. Research into WFE sensing and control has been extensively conducted for the Next Generation Space Telescope (NGST)[8].

In order to better understand the technological difficulties involved in designing and building a sparse aperture array, the challenge of building a Golay-3 interferometer satellite was undertaken. The MIT Adaptive Reconnaissance Golay-3

* sjchung@mit.edu; phone 617-253-6685; Graduate Research Assistant;MIT Space Systems Laboratory
** millerd@mit.edu; phone 617-253-3288; Associate Professor; Department of Aeronautics and Astronautics, MIT
*** deweck@mit.edu; phone 617-253-0255; Assistant Professor; Department of Aeronautics and Astronautics, MIT

Optical Satellite (ARGOS)[4] project exploits wide-angle Fizeau interferometer technology with an emphasis on modularity in the optics and spacecraft subsystems. The objective of the Adaptive Reconnaissance Golay-3 Optical Satellite (ARGOS) project is to demonstrate the practicality of a modular architecture for space-based optical systems.

Fig. 1 highlights the key functional and operational objectives. To demonstrate a complete spacecraft in a 1-g environ-

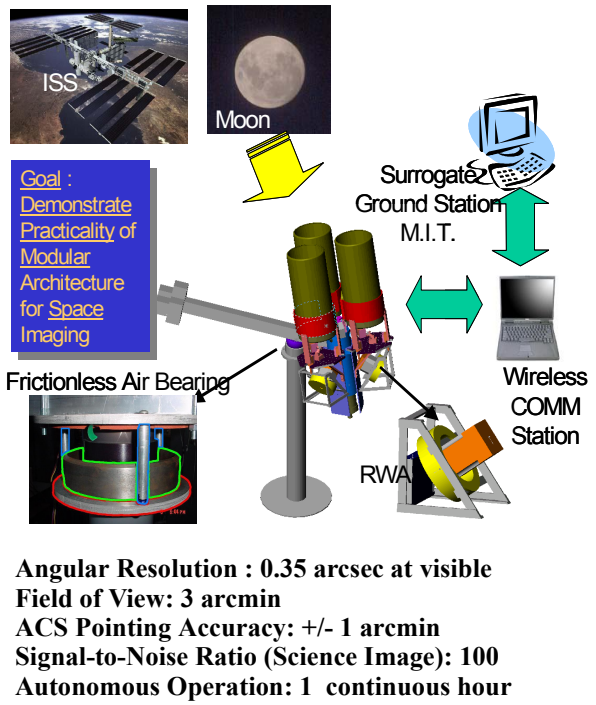

FIG. 1: Overview of ARGOS

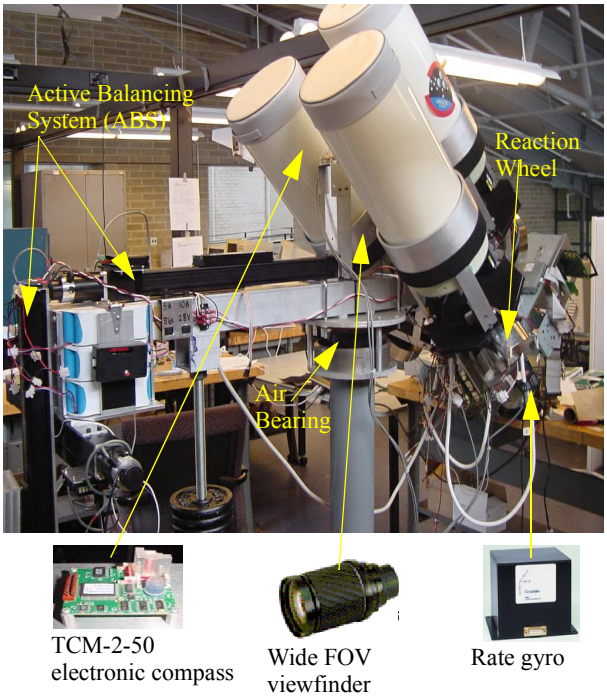

FIG. 2: The final ARGOS system with the three ACS sensors shown in the bottom

ment, the ARGOS system is mounted on a frictionless air-bearing, and has the ability to track fast orbiting satellites like the International Space Station (ISS) as well as point stars. Modular architecture design emphasizes the use of replicated components and quick connections. The system consists of three identical apertures arranged in a Golay-3 distribution. The light from these telescopes is combined in a center module and transmitted to a Charge-Coupled Device (CCD). Wavefront sensing techniques are explored to mitigate initial misalignment and to feed back real-time aberrations into the optical control loop. The goal is to obtain an image as good as the image received from a monolithic telescope using a single aperture. ARGOS operates autonomously and in a self-contained manner while a wireless ground station downloads images and telemetry information.

2. ANALYSIS OF SPARSE APERTURE INTERFEROMETRIC ARRAY

2.1 Determination of Array Configuration

Traditional image quality criteria such as resolution and encircled energy (EE) are inadequate for many sparse aperture or interferometric array applications[9]. When we look at extended objects such as the Moon and a faint distant nebula, evaluation of an optical system is far more complicated than by simply looking at a point source response (PSF). MTF is a better metric to evaluate the contrast (modulation) transfer characteristic of an extended object. In Fig. 3, the PSF and MTF plots of D=0.21m (ARGOS subaperture diameter) and L=0.12m (solid), 0.19m (dashdot), 0.3m (dotted) are shown. A

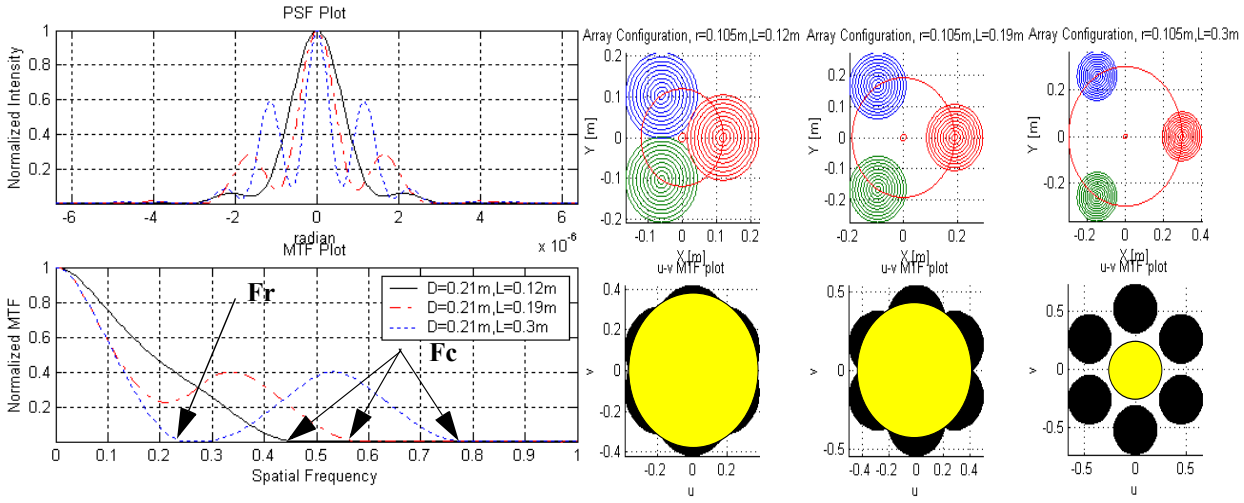

FIG. 3: PSF and MTF plots when D=0.21m and L = 0.12m (solid), 0.19m (dashdot), 0.3m (dotted). The corresponding array configurations are shown to the right of PSF-MTF plot. The black-yellow figure is a MTF plot. Yellow circles indicate the practical cut-off frequency.

perfect monolithic array, free of optical aberrations, has a linearly decreasing MTF contrast characteristic (See the solid MTF line of Fig. 3). In case of a sparse array, the MTF suffers a contrast loss in the mid spatial frequency range as shown in Fig. 3. We can see the MTF plot with L=0.3m exhibits two zero values rather than one. The first zero denoted by Fr is the practical spatial cut-off frequency, and defines the "practical resolution limit". The Fc is the cut-off frequency, whose inverse indicates an angular resolution under the normal condition that there is no Fr (another zero point) before Fc. So the larger Fc or Fr is, the better angular resolution a sparse array will achieve.

As opposed to a monolithic aperture, the method of Full-Width-Half-Maximum (FWHM) is not sufficient to determine the angular resolution. Assuming that angular resolution is fully determined by the array size, PSF can reveal the highest achievable angular resolution. This assumption holds especially for very large baseline Michelson interferometers. We can observe in Fig. 3, that the mainlobe size of the PSF plot is getting smaller, indicating improving angular resolution as we increase the array size L. The Fizeau interferometer, however, requires an instant full u-v coverage, which limits our practical resolution. In addition, as discussed above, the considerable contrast loss in the mid-spatial frequency range should be avoided. The angular resolution from the MTF plot of a Golay-3 type sparse imaging array is calculated by[4]

$$\theta_r = 1.22\frac{\lambda}{D_{eff}} = 2.44\frac{\lambda}{3L+\sqrt{4D^2-3L^2}} \quad . \tag{1}$$

As we increase L, the array becomes more sparse, which, as a result, boosts the heights of sidelobes on the PSF plots. The MTF plot of L=0.3m (dotted in Fig. 3) has two zeros while others have only one. It means the resolution is limited not by Fc but Fr, whose inverse is an angular resolution of one single aperture (1.22 * wavelength/D). So the sparse array has no advantage over one subtelescope. The array configuration of the ARGOS is selected as L = 0.19185 m for D=0.21 m subtelescopes, and it gives a better theoretical angular resolution of 0.35 arcsec rather than 0.55 arcsec for a single aperture, as well as a reasonable MTF characteristic.

2.2 Beam Combining Errors

There are three major wavefront errors that need to be controlled at the beam combiner in order to achieve phased beam combining. Those errors are Optical Path Difference (OPD), Tip/Tilt error, and pupil mapping error.

2.2.1 OPD (Piston) Error

We can plot the effects of OPD errors using the interferometry equation given by Mennesson[10].

$$I \propto \left| \frac{\pi D(1+\cos(r))}{\lambda} \right|^2 \left| \frac{J_1(\pi D \sin r/\lambda)}{\pi D \sin r/\lambda} \right|^2 \left| \sum_{k=1}^{n} e^{j2\pi(L_k r/\lambda)\cos(\delta_k - \theta)} e^{j\phi_k} \right|^2 . \quad (2)$$

where r is the off-axis angular direction, θ is the azimuth angle, D is a subaperture diameter ,and (L_k, δ_k) are the polar coordinates of the array configuration. ϕ_k is the phase shift.

As the piston error increases, two major deviations develop over the envelope of the PSF. First, the main envelope shifts in the direction of the piston error. The resultant direction of the envelope shift is the vector sum of piston error directions weighted by the amount of error. Secondly, the peak intensity gets reduced compared to the normal PSF without any piston errors resulting in a reduced Strehl Ratio (SR). The size of the mainlobe also expands showing a degraded angular resolution (See Fig. 4). When a piston error is 0.1λ, the peak intensity is 98% of the normal intensity. The beam combining piston error tolerance is 0.1λ = 55nm.

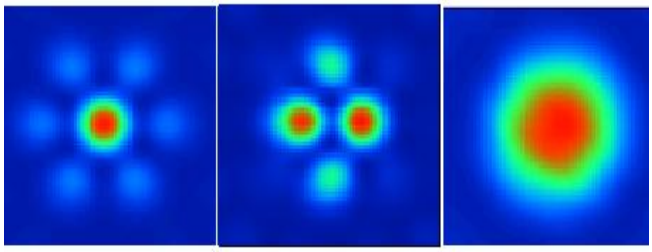

FIG. 4: PSF plot of Golay-3 array with zero OPD, 0.5 λ OPD , and 1.0 λ OPD, from the left to the right.

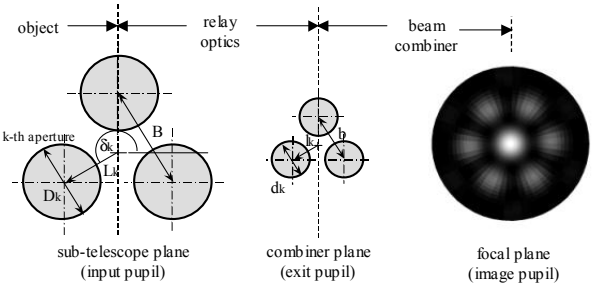

FIG. 5: The golden rule of beam combining, pupil mapping

2.2.2 Tip/Tilt Error

The approach employed here to analyze tilt errors is to further segment each aperture to smaller elements. Then we can imagine 3 aperture golay array consisting of numerous tiny apertures. The point spread function is calculated by summing up all the interference from each element. The phase difference at the central point due to tilt errors are added to the interference term of Equation (2). By reading the SR values of the PSF plots under the influence of tilt errors, the maximum allowable tilt error at the beam combining section is determined. This FEM method predicts the tilt tolerance between each beam entering the beam combiner should be less than 20 μ degrees (0.072 arcsec = 0.35 μrad).

2.2.3 Pupil Mapping Error

If coherent imaging is to be achieved over any significant FOV, the pupil mapping process must be performed such that the exit pupil is an exact (scaled) replica of the entrance pupil[3]. This constraint is commonly called the golden rule of beam combining. From the geometry of Fig. 5, Faucherre[5] derived the net OPD error due to the incorrect pupil mapping,

$$OPD_{net} = \left| B\sin\alpha - b\sin\beta \right| = \left| B\sin\alpha - \frac{B}{m_s}\sin(m_a\alpha) \right| . \quad (3)$$

The equation was developed to see the effect of both incorrect shear and incorrect magnification errors[4]:

$$\Delta l = \left| \frac{\lambda}{5\sqrt{3}FOV(m - \Delta m)} - \frac{\Delta m L}{m^2 - m\Delta m} \right| . \quad (4)$$

where Δl is the allowed shear error and Δm is the magnification tolerance for 0.1λ coherent phasing.

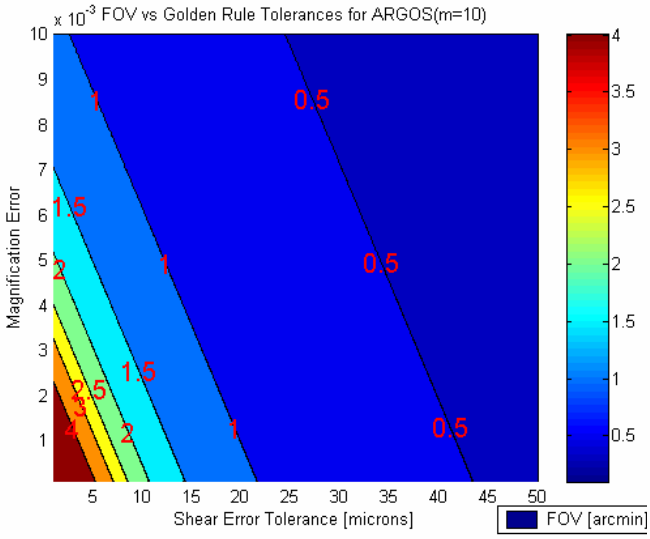

FIG. 6: FOV vs. Pupil mapping tolerances for ARGOS with achievable magnification tolerance

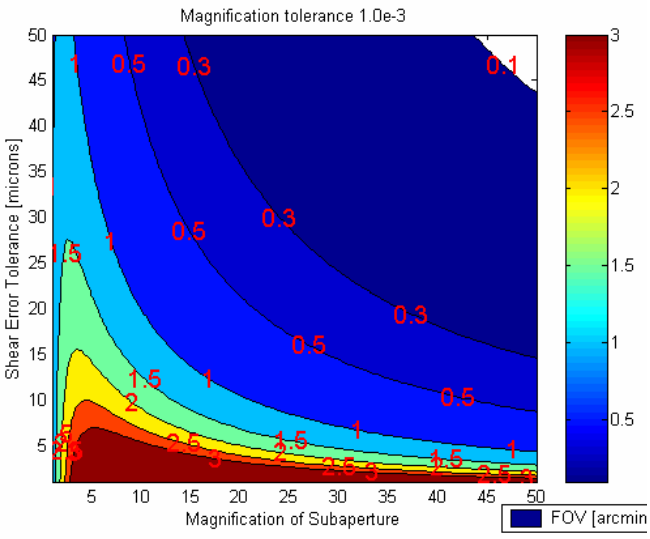

FIG. 7: Magnification vs. shear tolerance with magnification error =0.001

These results are graphically plotted in Fig. 6 and Fig. 7. Previously, 12µm was suggested for shear error tolerance with an assumption of no magnification error. However, 12µm shear error cannot produce the FOV requirement of ARGOS (3 arcmin) for any range of magnification error in Fig. 6. We can tighten shear error tolerance to meet the FOV requirement or we can relax the FOV requirement by shrinking the region of interest in the whole FOV. Therefore, the pupil mapping process is the primary limiting factor deciding the reasonable FOV of a sparse aperture interferometric array. ARGOS's sub-telescope collimators are designed with a tolerance of 0.0095. However, the ARGOS sub-telescopes have a focusing knob which can control the distance between the primary mirror and the secondary mirror, thereby controlling the size of the beam more precisely. It is usually considered that 1/1000 magnification tolerance requirement is too expensive to manufacture. Fig. 7 describes how the magnification of a sub-aperture affects the shearing tolerance of a sparse aperture imaging system. This plot implies that sub-aperture magnification can be tuned to maximize allowable shear error (lateral pupil mapping error) thereby reducing control complexity. For a magnification of 10, we can increase the shear tolerance value sufficiently high at the expense of the reduced FOV.

3. ARGOS OPTICS SYSTEM

3.1 Sub-Aperture

The overall cost of the ARGOS optics system could be significantly reduced by selecting one of the highest precision optics commercially off-the-shelf (COTS) telescope. However, it is necessary to customize a collimating lens to convert a Dall-Kirkham-type focal telescope to an afocal telescope with a magnification ratio of 10. The collimating lens is placed into the baffle of the telescope to make the system compact. A trade-off analysis was performed on several different cemented doublets that were optimized extensively by ZEMAX. One drawback of the cemented doublet is that it has bonded glasses, therefore if there is a change of temperature, the doublet may fail. Although a doublet with CaF2 performs best in reducing chromatic aberrations, the high CTE of CaF2 (18.3) forced us to find other glass combination for efficient achromatic doublet design. Smith[11] suggests FK51 (as a crown element) with a KzFS or LaK glass (as a flint). Although the maximum focal shift range can be minimized to 247 microns with FK51-KzFS11, it was not the best choice

due to the residual aberrations (RMS wavefront errors predicted by ZEMAX). The final FK51-BaK2 design achieves 271.6 micron chromatic focal shift range.

3.2 Design of OPD and Tilt/Tip Controller

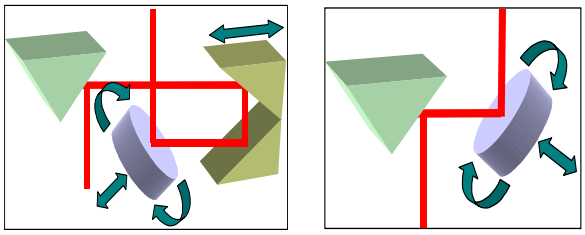

FIG. 8: Perpendicular ODL design with FSM (left) and Parallel ODL design coupled with FSM (right)

When strictly looking at two designs of optical delay lines (ODL) in Fig. 8, a perpendicular design seems to offer the most benefits. For the perpendicular design, a multi-axis FSM could be used to generate the required tip/tilt actuations as well as fine optical path difference control. FSM's have very fine resolutions so depending on them for fine OPD control will allow us to have a cheaper coarse control for the ODL. When the parallel ODL design is coupled with a FSM (Fig. 8), the resulting design is very simple and more cost-effective than the perpendicular design. This design cannot perform coarse OPD control, but this design is more compact resulting in easier integration with the structural design. In addition, there is no need for a translational stage or rooftop mirror which reduces the cost and control complexity, and there is also a greater total reflectance since there are fewer mirrored surfaces. Fewer mirrored surfaces also lead to fewer structural misalignment errors. In both the perpendicular ODL design and the parallel ODL design, fine OPD control is coupled with shear control so that ΔFine OPD = ΔShear. The effect that a change in fine OPD would have on shear, is not that great and could be ignored for adjustments < 10 microns. This is because we have a much tighter tolerance on piston error (50 nm) than a 12 micron shear error. A fine resolution multi-axis FSM from Physik Instrumente (PI), capable of controlling the tilt/tip as well as piston motion, was selected as ODL-FSM actuator of ARGOS.

3.3 Pyramidal Mirror and Beam Combiner

The pyramidal mirror turns all three beams 45 deg. into the beam combiner. A custom pyramidal mirror is chosen due to the cost of making one out of regular mirrors. The main reason for the high cost is that we would need to purchase special thin mirrors that cost $1000+, and then mount them to an accuracy of +/- 0.001° (+/- 3.6 arcsec). The pyramid cannot be made from the regular thickness mirrors since they constrain the beam diameter. We customized a pyramidal mirror with a surface accuracy of λ/10 peak to valley, +/- 3 arcsec angle error, and 50mm clear aperture. The substrate material is BK7 with a coating of AlSiO (aluminum with silicon monoxide). The reflectance will be approximately 90% in the visible range. The two point spread functions shown in Fig. 9 demonstrate how the FSM can compensate for the +/- 3 arcsec errors in the pyramid. In order to compensate for pyramid errors the FSM has to align itself so that the two reflecting surfaces are parallel.

Two options available for the beam combiner are either reflecting or refracting optics. The reflecting beam combiner is compact when compared to a refractor. Unfortunately, the secondary mirror of a Cassegrain telescope would partially block the three incoming beams in any possible configurations in order to obey the golden rule discussed in Sec. 2.2.3. A single parabolic mirror was considered, however there was not enough space between the pyramidal mirror. Had we used reflecting optics, there would be nothing available as COTS, therefore it would have to be custom manufactured increasing cost significantly. A reflector would also complicate the relay optics significantly since we would not be able to use the pyramidal mirror. In contrast, the refracting telescope has many advantages. It allows for very simple relay optics. It is

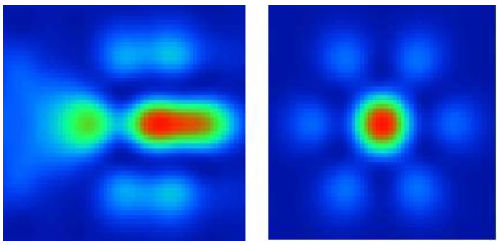

FIG. 9: The PSF simulation of the ARGOS with 3 arcsec tilt error of the pyramidal mirror (SR=0.444, Left). The PSF with FSM correction (SR=0.960, Right)

available COTS with high quality optics and is therefore relatively cheap. The FSQ-106N from Takahashi has been purchased. This telescope has significantly less chromatic aberration than other COTS telescopes. This is due to its four element design, two of which are fluorite. It has a diameter of 106 mm, and a 530 mm focal length, resulting in a total system focal length of 5300 mm.

3.4 Final Optical Layout

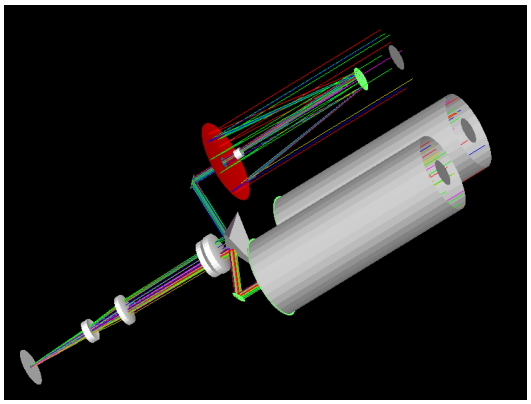

FIG. 10: 3D nonsequential ray-tracing using ZEMAX

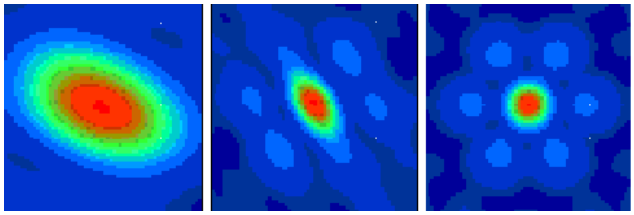

FIG. 11: The PSF plots when the beam combiner has tilt errors. From left to right, (1) X tilt: 0.2, Y tilt: 0.4 , (2) X: 0.3 Y: 0.3, (3) X: 0.25 Y: 0.25 [degrees]

The current optical layout of the system is as follows. Light shines in through the sub-aperture. The light continues through the telescope with a 210mm diameter until it hits the collimator which is inside the telescopes baffle. The light then goes through the collimating lens producing a 21mm diameter beam. The light exits and hits a reflecting mirror mounted onto a three axis FSM that acts as an ODL as well. The light is then reflected to the pyramidal mirror that is stationary. The light beam then enters the beam combiner, and is focused onto the CCD. The FSM has to be able to compensate for any errors in its mounting. Therefore a high precision mount with a range up to 7 degrees was selected for the FSM actuators (see Table 1). The pyramidal mount is composed of two stages. The first stage provides all of the angular adjustments and the second handles X & Y translation in the entrance pupil of the beam combiner. The X-Y translation stage is small enough to fit behind the tip/tilt rotation stage and has the load capacity to hold both the second stage and the mirror. Any additional Z directional error can be offset by the FSM mounts.

TABLE 1: Actuator and mount specifications

Model	Angular Range	Angular Resolution	Linear Range	Linear Resolution
FSM	± 600 μrad	± 0.05 μrad	12 μm	0.2 nm
FSM Mount	± 7 °	± 0.0008 ° (± 14 μrad)	1 cm	1 μm
Pyramid Mirror Mount	± 4 °	± 2 arcsec (± 9.6 μrad)	13 mm	3 μm

3.5 Structural Misalignment Tolerancing

Using the non-sequential ray tracing mode of ZEMAX, a complete ARGOS optics layout is constructed based on the optical specifications of a subaperture, pyramidal mirror, and the beam combining telescope as shown in Fig. 10. We intentionally perturb the sub-telescope or pyramidal mirror to determine allowable structural misalignment, and we compensate the tilt error by changing the tilt angle of the fold mirror attached to the FSM. At 0.01 degree tilt of a subaperture, a pure FSM motion cannot restore the SR (Strehl Ratio) above 0.8. But the addition of FSM piston motion can restore the SR value to 0.859. We can achieve a SR of 0.859 (which is above diffraction limited) over 0.01 degree tilt. But due to a magnification factor 10, the FSM compensation exceeds its max range (0.6 mrad=0.034 degree). Since we mounted a FSM onto a precision tip-tip mount which is capable of several arc-second adjustment (Table 1), this static error does not limit the FSM performance. However, it is safe to have a FSM within a range of eliminating a possible maximum alignment error. 0.005 degrees or 15 arcsec for sub-telescope structural misalignment is suggested. By assuming that all other optical components are perfectly aligned and the FSM can compensate all the residual tilt errors, the tilt errors for each surface of the pyramidal mirror are calculated. When the tilt error of the pyramidal mirror unit equals the tilt compensation of a FSM, the aberration loss due to the tilt is completely eliminated. Therefore there is no theoretical tilt tolerance for the pyramidal mirror as long as it does not exceeds the maximum compensation range (0.01 degrees). The beam combiner was tilted along x and y axis while leaving other optical components perfectly aligned (Fig. 11). This beam combiner misalignment is not correctable by optical actuators like FSMs. However, it turns out that we can tolerate up to 0.2 degrees for the beam combiner, which is less stringent than other misalignment tolerances.

4. SYSTEM COST MODELING

4.1 Replay Optics Cost Model

The three primary cost categories are the development of the spacecraft payloads and buses, deployment (i.e. launch) of the system, and the operation of the system. The cost of the sparse aperture payload can be further broken down into subapertures, the relay optics including beam combiner, and the CCD system. In order to derive the cost estimating relationships (CERs) of the relay optics portion of a sparse aperture array, identifying the theoretical relationships between the design parameters is considered. From the experience of building the optics control system of the ARGOS testbed, it is observed that the cost of the relay optics including beam combining control depends on the beam combining tolerances such as shearing error and tip/tilt error discussed in Sec. 2. The control difficulty caused by stringent beam combining tolerances defines the complexity of optics control actuators (ODLs and FSMs), and the quality of optics and structures. For example, if we have a tight beam combining requirement, the control actuator and actuator mount with a resolution smaller than this beam combining requirement is required, thereby increasing the cost.

Among three primary beam combining errors, the piston error requirement itself does not scale with any design parameters such as diameter of aperture or array size. In fact, derivations of tip/tilt errors and pupil mapping errors are based on the requirement of l/10λ phasing. A magnification tolerance of pupil mapping is assumed to be fixed at the manufacturable level. Then, the optics control effort becomes a function of tip/tilt and shearing error tolerances.

$$CER_{RelayOptics} \propto Control\_Effort = \frac{C_1}{Shear^A} + \frac{C_2}{Tilt^B} + \alpha. \quad (5)$$

We can also derive the tilt error tolerance as a function of a compressed beam size (d=D/m). Simplifying the FEM tilt analysis done in Sec. 2, the maximum allowable OPD error due to the relative tilt angle between two compressed beams

with a diameter of d is calculated. Additionally, the FOV of the system can be derived using the angular resolution element (Equation (1)) of the system multiplied by the number of CCD pixels (n). In Equation (5), we assume $C_1 = 1$ and $C_2 = 3$, based on the fact that one FSM needs three control channels to actively actuate three PZT stacks separated by 120 degrees for tip/tilt control. It was observed while building the ARGOS testbed that more control channels increase the cost. For example, three PZT amplifiers and three D/A channels are required for one single FSM as compared to one per each translational stage for shear or OPD control. The exponents, A, B of Equation (5) are assumed to be one indicating the control cost is inversely proportional to the tolerable values of shear error and tilt/tip error. Then, the control effort estimate becomes a function of the subaperture diameter (D), the array compactness (D/L) and m:

$$Control\_Effort = \left| D\frac{3+\sqrt{4(D/L)^2-3}}{12.2\sqrt{3}(m-\Delta m)n(D/L)} - \frac{\Delta m D}{(m^2-m\Delta m)(D/L)} \right|^{-1} + 3\left[\frac{\lambda m}{5D}\right]^{-1} \quad (6)$$

Equation (6) is plotted in Fig. 12 with n=1024, magnification =10, and magnification error, 1e-3. Five different values of

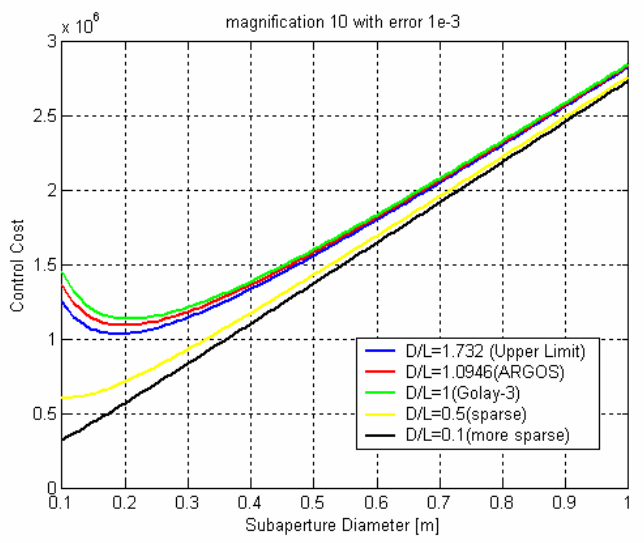

FIG. 12: Control cost vs. subaperture diameter for different array compactness

array compactness (D/L) have been selected. The blue line is the upper limit of D/L=1.732= $\sqrt{3}$, in which the individual telescopes touch each others (the most compact array). The red line corresponds to the ARGOS configuration with D=0.21m and L=0.19185m. The green line is the original Golay-3 configuration with D=L. The ratio of 1 is the minimum D/L with which no singular point is expected inside the MTF envelope as discussed in Sec. 2.1. The smaller values of D/L were also plotted to observe the control cost trends for longer baseline interferometers like Michelson interferometry. If the squared-root term in the effective diameter equation (Equation (6)) becomes imaginary, and the imaginary parts are ignored in this calculation. This means that the angular resolution of the effective diameter of long baseline interferometer is determined only by L. For a compact Fizeau type interferometry with D/L greater than 1, we can decrease the control cost by making the array more compact. It is interesting to note that there exists a minimum control cost point for a compact sparse array (D/L>1). This is because shear error dominates at small sub-aperture diameter region while tilt error dominates at large sub-aperture diameter. We can see that the second part of Equation (6) (tilt effect) is linearly proportional to D. As we further increase the array size, the system becomes more sparse, and the minimum control disappears

(moves to the negligible aperture size). However we can decrease the control cost by longer baselines. The subaperture diameter, 0.21m of ARGOS is near the minimum control point.

4.2 Quantitative Life-Cycle System Analysis

An analogy-based cost estimating approach is employed to derive the CERs of sparse array spacecraft systems. Based on

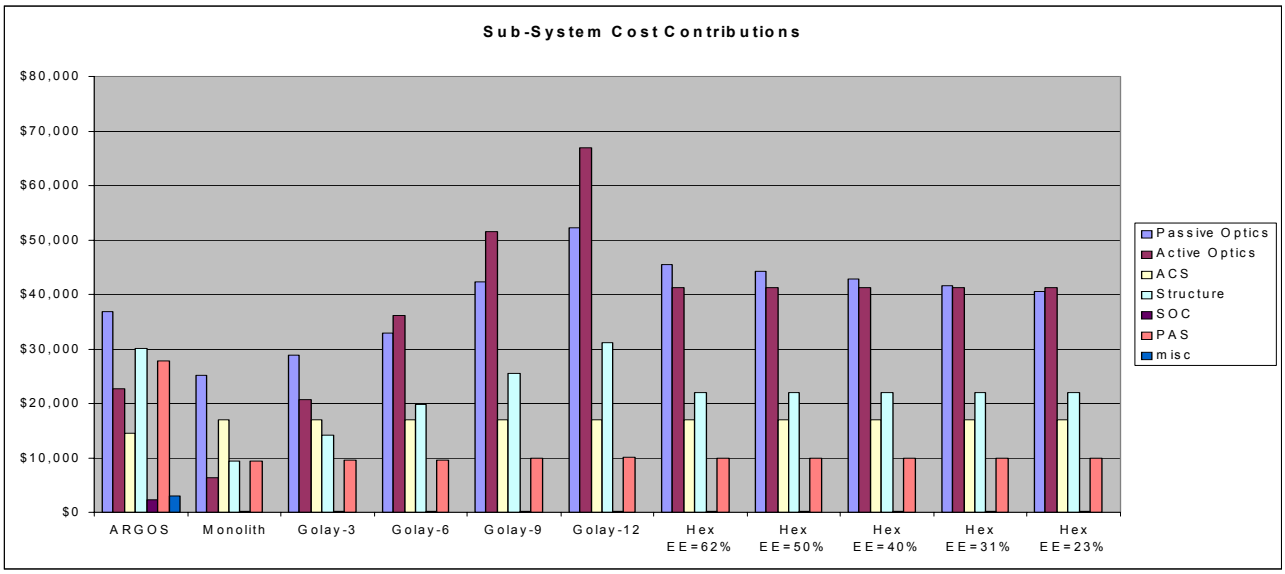

FIG. 13: Subsystem cost estimates for different array configurations. SOC means Science,Operation,Communication, and PAS Power,Avionics,Software subsystem. The active optics of Monolith represents target-tracking FSM control.

the detailed subsystem costs of the ARGOS, the CERs of the different configurations such as Golay-6, Golay-12 and the Hex arrays are developed. Nonrecurring and recurring items are identified and the CERs are adjusted for differences in size or complexity. Firstly, the scaling law of a monolithic telescope is used to calculate the subaperture diameter. In order to estimate the Attitude Control System (ACS) cost, regression was performed to derive the relationship between Reaction Wheel Assembly (RWA) mass and momentum capacity from the data collected from RWA manufacturers. The ACS cost scales with the RWA mass assuming the RWA mass dominates the ACS mass. The costs of other subsystems are adjusted by the same method. The labor cost is also taken into consideration by categorizing the subsystem members into management, staff, and engineer levels. Fig. 13 shows the resulting cost estimates for different sparse array configurations. We can observe that the labor costs dominate the hardware cost. Among the subsystems, the two optics groups are the major cost driving factor. Even though passive optics (telescopes and optics supply) dominate the cost for few subapertures, active optics subsystem (the relay optics, actuators, and WFE sensor) dominate the cost for many sub-apertures.

To see the effects of compactness on a Golay-3 type sparse aperture system, the CERs are developed as a function of effective diameter and array compactness as shown Fig. 15. Without the complex beam combining part (the relay optics cost in the previous section) of a sparse interferometric array, the telescope cost of monolithic apertures is higher than a sparse array as depicted in Fig. 14. Therefore, it is the relay optics that dominates the cost of a sparse array system. This cost analysis predicts emergence of a break-even point between monolithic systems and Golays. Past this break-even point, we can build a sparse array system with lower cost than a monolithic aperture system with the same effective diameter.

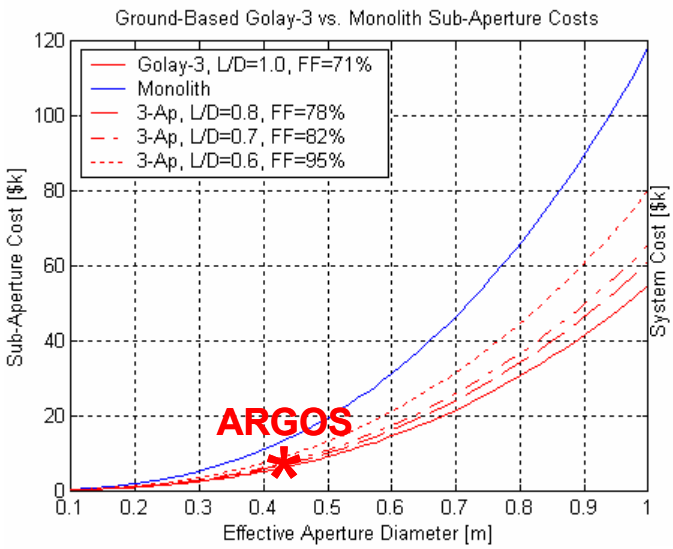

FIG. 14: Cost of telescopes for three-aperture array

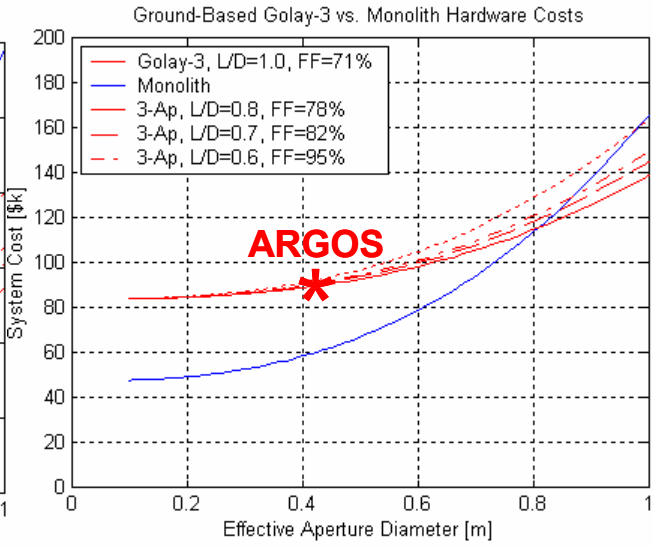

FIG. 15: System cost of three aperture array spacecraft

5. CONCLUSION

The ARGOS testbed is the first sparse aperture array simulating a space-borne observatory in a 1-g environment representing real world problems such as the vibrational coupling between a spacecraft structure and the wavefront errors propagating through the whole system. If ARGOS succeeds in coherent beam combining, it will be the first sparse aperture array to obtain a phased image of a real target in the sky. ARGOS is successfully designed and integrated into the full structure ready to operate. The optics controller utilizing model-based control and neural network is under development as well as software-based wavefront sensing techniques. A preliminary assessment shows that the beam combining problem is the most challenging aspect of sparse optical arrays. The need for optical control is paramount due to tight beam combining error tolerances. The wavefront sensing/control requirements appear to be a major technology and cost driver. The quantitative life-cycle cost model developed from the actual costs spent on the ARGOS testbed predicts a break-even point between monolithic systems and sparse arrays validating the objective of building sparse interferometric arrays.

ACKNOWLEDGEMENTS

This research was supported by the NRO Director's Innovation Initiative (DII) under contracts number, NRO-000-01-C-0207.

REFERENCES

1. A.B. Meinel, "Cost Scaling Laws Applicable to Very Large Telescopes", SPIE Proceedings Vol. 172, 1979.
2. M. Golay, "Point Arrays Having Compact Non-redundant Autocorrelations", J.Opt Soc. Am., vol. 61, pp 272, 1971.
3. J.E. Harvey, P.R. Silverglate, and A.B. Wissinger, "Optical Performance of Synthetic Aperture Telescope Configurations", Southwest Conference in Optics, pp 110-118, SPIE vol. 540, 1985.
4. S.-J. Chung, "Design, Implementation and Control of a Sparse Aperture Imaging Satellite", Master of Science Thesis, Department of Aeronautics and Astronautics, MIT, 2002.
5. M. Faucherre, F. Merkle, and F. Vakili, "Beam Combination in Aperture Synthesis from Space: Field of View Limitations and (u,v) Plane Coverage Optimization", New Technologies for Astronomy, pp 138-145, SPIE vol. 1130, 1989.
6. C.R. De Hainaut, et al, "Wide Field Performance of a Phased Array Telescope", Optical Engineering, vol. 34 No.3, March 1995.

7. V. Zarifis, et al, " The Multi Aperture Imaging Array", ASP Conf. Series 194, Working on the Fringe: Optical and IR Interferometry from Ground and Space, Unwin and Stachnik, eds, pp. 278.
8. D.C. Redding, et al, “Wavefront sensing and control for a Next-Generation Space Telescope”, Proc. SPIE Vol. 3356, p. 758-772, 1998.
9. J.E. Harvey, and R.A. Rockwell, "Performance Characteristics of Phased Array and Thinned Aperture Optical Telescopes", Optical Engineering, Vol. 27 No.9, September 1988.
10. B. Mennesson, and J.M. Mariotti, " Array Configurations for a Space Infrared Nulling Interferometer Dedicated to the Search for Earthlike Extrasolar Planets", ICARUS 128, pp 202-212, 1997.
11. W.J. Smith, *Modern Optical Engineering*, 3rd ed, McGraw-Hill, 2000.